MATHEMATICAL BIOSCIENCES
AND ENGINEERING
Volume **7**, Number **2**, April **2010**

doi:10.3934/mbe.2010.7.237

pp. **237–258**

MORPHOLOGICAL SPATIAL PATTERNS IN A REACTION DIFFUSION MODEL FOR METAL GROWTH

Benedetto Bozzini

Dipartimento di Ingegneria dell'Innovazione, Università del Salento - Lecce
via per Monteroni, I-73100 Lecce, Italy

Deborah Lacitignola

Dipartimento di Scienze Motorie e della Salute, Università di Cassino
Campus Folcara, Loc. S.Angelo, I-03043 Cassino, Italy

Ivonne Sgura

Dipartimento di Matematica, Università del Salento - Lecce
via per Arnesano, I-73100 Lecce, Italy

(Communicated by Stephen Gourley)

Abstract. In this paper a reaction-diffusion system modelling metal growth processes is considered, to investigate - within the electrodeposition context- the formation of morphological patterns in a finite two-dimensional spatial domain. Nonlinear dynamics of the system is studied from both the analytical and numerical points of view. Phase-space analysis is provided and initiation of spatial patterns induced by diffusion is shown to occur in a suitable region of the parameter space. Investigations aimed at establishing the role of some relevant chemical parameters on stability and selection of solutions are also provided. By the numerical approximation of the equations, simulations are presented which turn out to be in good agreement with experiments for the electrodeposition of Au-Cu and Au-Cu-Cd alloys.

1. **Introduction and the model.** Pattern formation is widely observable in nature: fish and animal coat markings, sand dunes, grass landscapes are just few of the many examples around us. The fascinating idea that these so different natural scenarios might be explained within a common theoretical framework is maybe one of the most striking features of pattern formation. For many years, a great effort has been devoted to understand and describe the constitutive mechanisms underlying such kind of processes, giving birth to stimulating researches in the field of nonlinear dynamics.

As shown by a large amount of theoretical and experimental literature, by the pioneering paper of Turing [34], many reaction-diffusion systems have been proposed to account for spatial pattern formation in chemistry, physics and biology [30, 26, 27]. Turing stressed the mechanism by which two reacting and diffusing chemicals, could induce spatial patterns in chemical concentrations from initial

2000 *Mathematics Subject Classification.* 35K57, 62P30, 65M.

Key words and phrases. Turing instability, pattern formation, electrodeposition, numerical simulations.

near-homogeneity. This phenomenon is now well known as diffusion-driven instability. At this regard, chemistry provides many examples: experimental results show striped and spotty pattern formations, as well as more complicated patterns [25].

In the electrochemical context, electrodeposition of Au alloys from cyanocomplex baths has been shown to exhibit electrokinetic instabilities that can lead to compositional heterogeneity in the electrodeposit bulk [1]. Such instabilities derive from a hysteretic current-voltage characteristic related to the buildup of CN^- concentration in the catholyte and attending variations the Cu(I)-cyanocomplex nobility [5]. In this paper we consider a model coupling the surface morphology and CN^- concentration, in order to rationalise the formation of the morphological patterns sometimes developing in electrodeposition (ECD). This phenomenon is a special case, original within the realm of metal electrochemistry, of a more general, well-known type of chemical and electrochemical dynamics (electrocatalysis [22], corrosion of Cu [20], Fe-group metals [22] and Ag [8]). To qualitatively describe such dynamics, we consider a simple model based on a reaction-diffusion approach, which has been shown to be able to capture the essential features of pattern development observed in experiments. A detailed presentation of a class of models including this one as a particular case, with full discussion of the underlying physics, is reported in [7]. The proposed model reveals a surprisingly rich phenomenology. In [9] the electrodeposit surface was regarded as isotropic in the substrate plane, a 1D model in space was considered and the initiation of spatial patterns induced by diffusion was shown. In [10], electrodeposition from cyanocomplex baths containing free cyanide was taken into account and shown to exhibit the existence of travelling wave solutions, corresponding to transition front waves, sometimes occurring in the experiments.

In this paper, we consider the electrodeposition model proposed in [7, 9] under the more realistic hypothesis of a 2D model in space, in order to obtain more suitable comparisons with the experiments. Investigations aimed at establishing the role of relevant chemical parameters on the system dynamics, are also performed.

We present a theoretical study of the model, its numerical approximation and some comparisons between simulations and electrochemical experiments. To the aim of completeness, we now briefly recall the model derivation proposed in [7, 9]. We stress that one chemical species adsorbed at the surface of the growing cathode is addressed, so that we deal with a system of two reaction-diffusion equations, one for *the morphology* and one for *the chemistry*. The equation for the morphological dynamics is:

$$\frac{\partial \eta}{\partial \tau} = D_s^* \Delta \eta + S^*, \tag{1}$$

with

$$S^* = \alpha_1 \frac{\eta^2}{1+\eta} - \beta_1 \eta \theta.$$

and $\Delta = \dfrac{\partial^2}{\partial x^2} + \dfrac{\partial^2}{\partial y^2}$. Here $\eta(x, y, \tau)$ is the dimensionless electrode shape (i.e. the intersection of the electrodeposit surface with a plane normal to the substrate), x and y are the dimensionless space coordinates, τ is the dimensionless time and D_s^* is the dimensionless surface diffusion coefficient of adatoms. In the source term S^*, $\theta(x, y, \tau)$ is the surface coverage with the adsorbed chemical species, the parameters α_1 and β_1 are strictly positive and weight the two terms in S^* accounting for: (i) localization of the ECD process and (ii) effects on the ECD rate of surface

chemistry, i.e. the presence of adsorbates at the growing cathode, respectively. The presence of adsorbable species in the ECD bath gives rise to the fact that $\theta(x, y, \tau)$ develops at a growing electrochemical interface as a function of space and time. $\theta(x, y, \tau)$ is controlled by the nature of the adsorbable species and of the surface active sites. The surface coverage dynamics can be described, as customary in chemical kinetics, in terms of a material balance with a source term containing positive and negative contributions related to adsorption and desorption. More precisely, the dimensionless form for the surface chemical dynamics can be expressed as:

$$\frac{\partial \theta}{\partial \tau} = D^*_{sc}\Delta\theta + S^*_c, \tag{2}$$

where D^*_{sc} is the surface diffusion coefficient of $CN^-$and S^*_c is the chemical source term, given by

$$S^*_c = K^*_{ADS}(\eta, \theta)(1 - \theta) - K^*_{DES}(\eta, \theta)\theta$$

where K^*_{ADS} and K^*_{DES} represent the adsorption and desorption rate constants, respectively.

By coupling equations (1) and (2), one obtains the following model in dimensionless form:

$$\begin{cases} \dfrac{\partial \eta}{\partial \tau^*} = \Delta\eta + \rho f(\eta, \theta), \\ \dfrac{\partial \theta}{\partial \tau^*} = d\Delta\theta + \sigma g(\eta, \theta), \end{cases} \tag{3}$$

with

$$f(\eta, \theta) = \frac{\epsilon\eta^2}{1 + \eta} - \eta\theta, \qquad g(\eta, \theta) = K^*_{ADS}(\eta, \theta) - [K^*_{ADS}(\eta, \theta) + K^*_{DES}(\eta, \theta)]\theta, \tag{4}$$

which is defined for $(x, y, \tau^*) \in [0, L_1] \times [0, L_2] \times [0, T]$, with L_1, L_2 characteristic lengths of the electrode, T a characteristic time of the electrodeposition process, and

$$\tau^* = D^*_s\,\tau, \qquad d = \frac{D^*_{sc}}{D^*_s}, \qquad \epsilon = \frac{\alpha_1}{\beta_1}, \qquad \sigma = \frac{1}{D^*_s}, \qquad \rho = \frac{\beta_1}{D^*_s}.$$

We also require (3) to be equipped with zero-flux boundary conditions and the following initial conditions:

$$\eta(x, y, 0) = \eta_0, \qquad \theta(x, y, 0) = \theta_0, \qquad (x, y) \in [0, L_1] \times [0, L_2]\,.$$

Motivated by experimental evidence, it is possible to explicitly choose the adsorption and desorption rates, in the following form:

$$K^*_{ADS} = A\exp(a\eta + b\theta), \qquad K^*_{DES} = A_1\exp(a_1\eta + b_1\theta), \tag{5}$$

where A, A_1, a, a_1, b, b_1 are positive parameters. More precisely, we consider the case, $A \neq A_1$, $a \neq a_1$, $b = b_1$, and choose $a_1 = a + \epsilon\ln\left(\dfrac{A}{\epsilon A_1}\right)$ and $\dfrac{A}{A_1} = \dfrac{\epsilon}{2}$. As a consequence, the reaction terms specialize as:

$$f(\eta, \theta) = \frac{\epsilon\eta^2}{1 + \eta} - \eta\theta, \qquad g(\eta, \theta) = A\exp(a\eta + b\theta)\frac{(\epsilon - \theta\epsilon - \theta 2^{1-\epsilon\eta})}{\epsilon}. \tag{6}$$

The rest of the paper is organized as follows: in Section 2, we will perform an analytical study of the homogeneous equilibria of the PDE system (3)-(6) and show the occurrence of a subcritical Hopf bifurcation for the model, stressing the role of

the parameter A on the stability properties of the non trivial homogeneous equilibrium. Next, in the Section 3 we deal with Turing instability: namely, we apply linear stability analysis to investigate the reaction-diffusion system, obtaining a set of conditions - in terms of the model parameters - that guarantee the initiation of spatial patterns induced by diffusion. Hence, we deal with the numerical approximation of the equations and, by means of the numerical simulations, we outline the role of the parameter a to control the pattern selection. Accordingly, we present representative simulations of pattern formations, that are shown to be in good qualitative agreement with some electrodeposition experiments.

2. **Homogeneous equilibria: A phase space analysis.** The spatially independent equilibria for model (3) are the solutions of the following system:

$$\begin{cases} \eta_e\theta_e = \dfrac{\epsilon\eta_e^2}{1+\eta_e} \\ K_1(\eta_e,\theta_e) = \theta_e K_2(\eta_e,\theta_e), \end{cases}$$

where $K_1(\eta,\theta) = K^*_{ADS}(\eta,\theta)$ and $K_2(\eta,\theta) = K^*_{ADS}(\eta,\theta) + K^*_{DES}(\eta,\theta)$.

In the present case, we focus on the two homogeneous equilibria:

$$E_1 = \left(0, \frac{A}{A+A_1}\right) = \left(0, \frac{\epsilon}{\epsilon+2}\right), \qquad E_2 = \left(\frac{1}{\epsilon}, \frac{\epsilon}{\epsilon+1}\right), \tag{7}$$

which turn out to have a certain relevance for the system dynamics.

As usual, to investigate the stability properties of the homogeneous steady states, we consider the Jacobian matrix of (3):

$$J(\eta,\theta) = \begin{pmatrix} \rho f_\eta & -\rho f_\theta \\ \sigma(K_{1\eta} - \theta K_{2\eta}) & \sigma(K_{1\theta} - \theta K_{2\theta} - K_2) \end{pmatrix}$$

where:

$$f_\eta = 2\,\frac{\epsilon\,\eta}{1+\eta} - \frac{\epsilon\,\eta^2}{(1+\eta)^2} - \theta; \quad f_\theta = -\eta; \quad K_{1\eta} = aAe^{(a\eta+b\theta)}; \quad K_{1\theta} = bAe^{(a\eta+b\theta)};$$

$$K_{2\eta} = K_{1\eta}\frac{a\epsilon + 2^{(1-\epsilon\,\eta)}\,(a - \epsilon ln2)}{a\epsilon}; \qquad K_{2\theta} = K_{1\theta}\frac{\left(\epsilon + 2^{(1-\epsilon\,\eta)}\right)}{\epsilon}.$$

2.1. **The trivial equilibrium E_1.** As far as the trivial equilibrium E_1 is concerned, the two eigenvalues of the Jacobian matrix $J(E_1)$ are both real and negative, i.e.

$$\lambda_1 = -\frac{\epsilon}{\epsilon+2}; \qquad \lambda_2 = -A\,\frac{\epsilon+2}{\epsilon}\exp\left(\frac{b\epsilon}{\epsilon+2}\right).$$

The spatially independent equilibrium E_1 is thus always a stable node. This is perfectly consistent with the chemical problem we are dealing with. In fact, the stability of equilibrium E_1 has a straightforward physico-chemical interpretation.

At such equilibrium, the condition $\eta_e^* = 0$, implies that the two equations in (3) are decoupled. Thus, the two equations can be studied separately.
The condition $\eta_e^* = 0$ corresponds to the absence of electrodeposit growth. From the physical point of view, this implies that the following electrochemical equation

$$Au(CN)_2^- + e^- \longleftrightarrow Au + 2CN^-, \tag{8}$$

corresponding to the formation of Au atoms, is at equilibrium. Here and in the rest of the paper for chemical expressions $(\cdot)$ indicates the name of the chemical substance and $[\cdot]$ the related concentration. The equilibrium of the electrochemical reaction expressed by (8) can be viewed as:

$$\begin{aligned} \vec{\nu} &= \vec{k} \cdot \left[Au(CN)_2^-\right] \cong \alpha \cdot \left[Au(CN)_2^-\right] \cdot \exp\left(\frac{-\eta}{B_c}\right) \\ \overleftarrow{\nu} &= \overleftarrow{k} \cdot [Au] \cdot [CN^-]^2 \cong \beta \cdot [Au] \cdot [CN^-]^2 \cdot \exp\left(\frac{\eta}{B_a}\right) \end{aligned} \tag{9}$$

where α, β, B_c and B_a are constants. At equilibrium the rates $\vec{\nu} = \overleftarrow{\nu}$ and then $\dfrac{\left[Au(CN)_2^-\right]}{[Au] \cdot [CN^-]^2} = \dfrac{\beta}{\alpha}$.

Similarly, $\theta_e^* = \dfrac{A}{A + A_1}$, corresponds to the adsorption equilibrium of CN^- onto active sites of the Au surface, that we denote Au^*. This chemical equilibrium can be expressed by the reaction

$$CN^- + Au^* \longleftrightarrow Au^* - CN^-_{ads} \tag{10}$$

and in terms of kinetic expressions as:

$$\begin{aligned} \vec{\nu} &= \vec{k} \cdot (1 - \theta) \cdot [CN]^- \\ \overleftarrow{\nu} &= \overleftarrow{k} \cdot \theta \end{aligned} \tag{11}$$

Again the equilibrium condition $\vec{\nu} = \overleftarrow{\nu}$ can thus be written as:

$$\theta_e^* = \frac{\vec{k}\,[CN^-]}{\vec{k}\,[CN^-] + \overleftarrow{k}} = \frac{\tilde{A}\,[CN^-] \exp(b\theta^*)}{\tilde{A}\,[CN^-] \exp(b\theta^*) + A_1 \exp(b_1\theta^*)}$$

We stipulated to consider the case: $b = b_1$ and $\tilde{A}\,[CN^-] = A$, whence $\theta_e^* = \dfrac{A}{A + A_1}$. A physico-chemical interpretation of the stability of the equilibrium E_1 thus boils down to the separate discussion of the stability of the equilibria expressed by equations (8) and (10). The stability of equation (10) is a special case of the stability of chemical reactions, that can be dealt with within the framework of the Gibbs-Duhem stability theory (see, e.g. [17] p. 49). The Gibbs-Duhem criterion can be restated in terms of chemical potentials and electrochemical dissipation. Such a criterion can be specialized to the relevant case as follows:

$$\frac{\partial \mu(Au^*)}{\partial \xi} + \frac{\partial \mu(CN^-)}{\partial \xi} - \frac{\partial \mu(AuCN)}{\partial \xi} < 0 \tag{12}$$

where $\mu(s)$ is the chemical potential of the chemical species s and ξ the degree of advancement of the reaction. Since for equation (10): $\dfrac{\partial \mu(AuCN)}{\partial \xi} > 0$, $\dfrac{\partial \mu(Au^*)}{\partial \xi} < 0$ and $\dfrac{\partial \mu(CN^-)}{\partial \xi} < 0$, then inequality (12) is always satisfied.

The stability of equation (8), expressing an electrochemical reaction, has not been discussed explicitly in the literature, but can be derived straightforwardly from the Gibbs-Duhem theory, mentioned above. In the case of interest, the electrochemical Gibbs-Duhem criterion reads:

$$\frac{\partial \mu(AuCN_2)}{\partial \xi} - \frac{\partial \mu(Au)}{\partial \xi} - 2\frac{\partial \mu(CN^-)}{\partial \xi} + F\frac{\partial \eta}{\partial \xi} < 0 \tag{13}$$

where F is the Faraday constant. Since for equation (8): $\frac{\partial \mu(AuCN_2)}{\partial \xi} < 0$, it follows $\frac{\partial \mu(Au)}{\partial \xi} > 0$, $\frac{\partial \mu(CN^-)}{\partial \xi} > 0$. As the process is a cathodic one, $\frac{\partial \eta}{\partial \xi} < 0$. Inequality (13) is thus always verified.

2.2. **The non trivial equilibrium E_2.** At the nontrivial homogeneous equilibrium E_2, the Jacobian matrix $J(E_2)$ is given by:

$$J(E_2) = \begin{bmatrix} \frac{\rho\,\epsilon^2}{(\epsilon+1)^2} & -\frac{\rho}{\epsilon} \\ \frac{\sigma\,Ae^{\alpha_0}\epsilon\,\ln 2}{\epsilon+1} & -\frac{\sigma\,Ae^{\alpha_0}\,(\epsilon+1)}{\epsilon} \end{bmatrix} \tag{14}$$

with $\alpha_0 = \frac{a\epsilon + a + b\epsilon^2}{\epsilon\,(\epsilon+1)}$. This leads to the characteristic equation: $\lambda^2 + B_1\lambda + B_0 = 0$, where

$$B_1 = \frac{A\sigma e^{\alpha_0}(\epsilon+1)^3 - \rho\epsilon^3}{\epsilon(\epsilon+1)^2}; \qquad B_0 = \frac{(\ln 2 - \epsilon)\,\rho\,\sigma\,Ae^{\alpha_0}}{\epsilon+1}. \tag{15}$$

In the following, we assume $\epsilon < \ln 2$. We also observe that the two roots of the characteristic equation can be expressed as $\lambda_{1/2} = \widetilde{\alpha}(A) \pm i\widetilde{\beta}(A)$ where:

$$\widetilde{\alpha}(A) = \frac{1}{2}\left(\frac{\rho\,\epsilon^2}{(\epsilon+1)^2} - \frac{\sigma\,Ae^{\alpha_0}\,(\epsilon+1)}{\epsilon}\right); \qquad \widetilde{\beta}(A) = \sqrt{detJ(E_2) - \widetilde{\alpha}^2}.$$

The quantity $detJ(E_2) - \widetilde{\alpha}^2$ may be expressed as $C_2A^2 + C_1A + C_0$, with:

$$C_2 = -\frac{\sigma^2\,(e^{\alpha_0})^2\,(\epsilon+1)^2}{4\epsilon^2} < 0; \quad C_1 = \frac{\sigma\,\rho\,e^{\alpha_0}\,(-\epsilon + 2\,\ln 2)}{2(\epsilon+1)}; \quad C_0 = -\frac{\rho^2\epsilon^4}{4\,(\epsilon+1)^4}.$$

Moreover,

$$C_1^2 - 4C_0C_2 = \frac{\rho^2\sigma^2 e^{2\,\alpha_0}\ln 2\,(\ln 2 - \epsilon)}{(\epsilon+1)^2}.$$

Since $\epsilon < \ln 2$, the quantity $C_1^2 - 4C_0C_2$ is always positive and $detJ(E_2) - \widetilde{\alpha}^2 > 0$ for every value of the parameter $A \in (A_1, A_2)$ where

$$A_{1,2} = \frac{\left(-\epsilon + 2\,\ln 2 \mp 2\sqrt{-\epsilon\,\ln 2 + (\ln 2)^2}\right)\epsilon^2\rho}{(\epsilon+1)^3\,e^{\alpha_0}\sigma}.$$

Therefore, the eigenvalues λ_1 and λ_2, have negative real part if

$$A > A_c; \qquad A_c = \frac{\rho}{\sigma}\frac{\epsilon^3}{e^{\alpha_0}\,(\epsilon+1)^3} > 0. \tag{16}$$

Since $\epsilon < \ln 2$, it follows through straightforward algebra, that $A_1 < A_c < A_2$. When $A = A_c$, the pair of complex conjugate eigenvalues crosses the imaginary axis, i.e. $\widetilde{\alpha}(A_c) = 0$. Furthermore, since the transversality condition

$$\frac{d\widetilde{\alpha}}{dA}(A_c) = -\frac{\sigma}{2}\,\frac{e^{\alpha_0}\,(\epsilon+1)}{\epsilon} \neq 0 \tag{17}$$

is verified, then by the Hopf bifurcation theorem [19] it follows that a family of periodic solutions bifurcates from the equilibrium E_2 when the bifurcation parameter A passes through A_c. By the means of numerical arguments, it is possible to show that, for $A > A_c$, the bifurcating periodic solutions are unstable.

The analysis above may be summarized as follows:

Theorem 2.1. *Assume $\epsilon < \ln 2$. Then:*
(i)The spatially homogeneous equilibrium E_2 is unstable if the parameter A is such that $A < A_c$ and it is asymptotically stable otherwise, i.e. when (16) holds.
(ii) When the parameter A is such that $A = A_c$, a Hopf bifurcation occurs.
(iii) The Hopf bifurcation is subcritical, i.e. the bifurcating periodic solutions exist for $A > A_c$ and are unstable.

The above result stresses the role of the parameter A for the occurrence of the Hopf bifurcation. Such a role is confirmed also from a chemical viewpoint. In fact, the quantity A describes the overall attachment efficiency of CN^- to the bare Au surface sites. As already noticed, A can be viewed as $A = \tilde{A}\cdot[CN^-]$. It thus contains two contributions: $[CN^-]$ describes the amount of reagent available for attachment to the surface, $\tilde{A}$ quantifies the affinity of the clean Au surface for CN^-. The condition $A < A_c$ has a straightforward physical interpretation: since the chemically stabilising factor is the coverage of the Au surface with CN^-, if the attachment efficiency A is below a threshold A_c - dictated by both material properties and reaction rate, giving rise to accumulation of CN^- - the growth dynamics is enhanced (for the case of CN^- adsorbed onto Au see [2, 3, 4]). Unless specific levellers are added to the electrodeposition bath, an increase of electrodeposition rate correlates with morphological instability (see, e.g. [33]).

To have a phenomenological picture of the above bifurcation analysis, we choose $\epsilon = 0.5$, $\rho = 40$, $\sigma = 2$, $a = 1$, $b = 1$ and consider A as a bifurcation parameter. In this case, the spatially homogeneous equilibria are: the equilibria E_1, E_2 as defined above and another equilibrium E_u. It is easy to prove that E_u is always unstable and has no role for the system dynamics. The equilibrium E_1 is always a stable node, whereas E_2 changes its stability when the parameter A is varied, because of a subcritical Hopf bifurcation occurring at $A = A_c = 0.071833$. More precisely, the following table resumes all possible scenarios:

Equilibrium	$A < A_1$	$A_1 < A < A_c$	$A_c < A < A_2$	$A > A_2$
$E_1 \equiv (0, 0.2)$	stable node	stable node	stable node	stable node
$E_2 \equiv (2, 0.33)$	unstable node	unstable focus	stable focus	stable node

As shown in the previous table, at $A_1 = 0.022194$ a node-focus transition occurs whereas at $A_2 = 0.23246$, a focus-node transition happens. Furthermore, $A_c = 0.071833$ is a Hopf bifurcation value and, according to the Hopf theorem, when A is increased above A_c, an unstable periodic orbit O_{E_2} appears around E_2. We stress also that while for $A < A_c$ the equilibrium E_1 turns out to be the only attractor for the system trajectories, when $A > A_c$ a bistability situation comes out, as shown in Fig.1

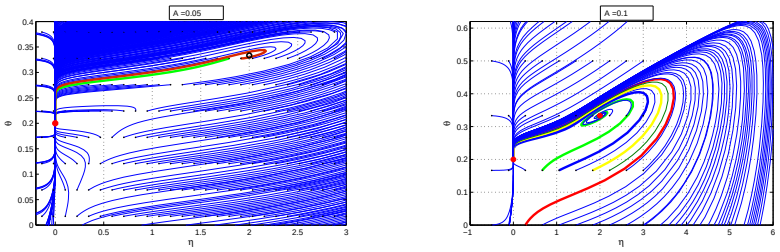

(a) (b)

FIGURE 1. The spatially independent case. System trajectories in the phase plane (η, θ) when the parameter A is varied. Red full circle denotes the equilibrium stability; blue empty circle denotes the equilibrium instability; dark dots denote the chosen initial conditions (a) The case $A < A_c$, i.e. $A = 0.05$: the equilibrium E_1 is the only attractor (b) The case $A > A_c$, i.e. $A = 0.1$ and the same initial conditions of case (a): a *bistability* situation appears.

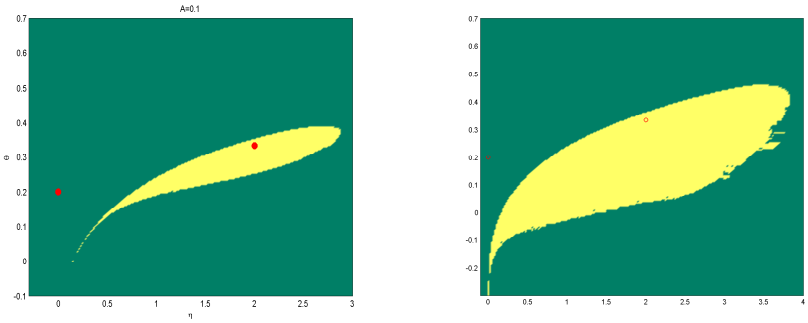

(a) (b)

FIGURE 2. The spatially independent case. The case $A > A_c$: *the basins of attraction* of the two homogeneous equilibria are separated by the unstable periodic orbit O_{E_2}. The *green* region represents the basin of attraction related to the homogenous equilibrium E_1; the *yellow* region represents the basin of attraction related to the homogenous equilibrium E_2; red full circle denotes the equilibrium stability. The basin of attraction of the equilibrium E_2, exhibits a strong dependence on the parameter A. (a) The case $A = 0.1$ (b) The case $A = 0.12$

In this range of the parameter A, the asymptotic behaviour of the system trajectories will thus strictly depend on the choice of the initial conditions: there are two different *basins of attraction* which are separated by the unstable periodic orbit O_{E_2}. Extensive numerical simulations show that the basin of attraction of E_2, becomes notably larger by increasing, even slightly, the value of the parameter A, as shown Fig.2. Such a circumstance also plays a certain role in the arising of spatial patterns for model (3) when diffusive processes are considered. These aspects will be investigated in the Section 3.

2.3. **A priori bounds for positive steady-state solutions.** In this section we provide some a priori bounds for the positive steady-state solutions of model (3). The related steady-state problem is:

$$\begin{cases} \Delta\eta + \rho\left(\dfrac{\epsilon\eta}{1+\eta} - \theta\right)\eta = 0, \quad z \in \Omega \\ d\Delta\theta + \sigma A \exp(a\eta + b\theta)\left(1 - \theta - \dfrac{\theta 2^{1-\epsilon\eta}}{\epsilon}\right) = 0, \quad z \in \Omega \\ \dfrac{\partial\eta}{\partial n} = \dfrac{\partial\theta}{\partial n} = 0, \quad z \in \partial\Omega \end{cases} \tag{18}$$

where $z = (x, y)$; $\Omega = (0, L_1) \times (0, L_2)$. Let (η, θ) be an arbitrary positive solution of (18). To get some a priori bounds on such solution, we will use two classical results from the elliptic theory of partial differential equations, that is the Harnack Inequality [23] and the Maximum Principle [24], as applied in the context of reaction-diffusion systems. First of all, a direct application of the Maximum Principle Theorem [24] to (18.2), gives $\theta \leq 1$ on $\bar{\Omega}$.
On the other hand, we rewrite (18.1) as

$$\begin{aligned} &\Delta\eta + c(z)\eta = 0, \quad z \in \Omega \\ &\frac{\partial\eta}{\partial n} = 0, \quad z \in \partial\Omega, \end{aligned}$$

where $c(z) = \rho\left(\dfrac{\epsilon\eta}{1+\eta} - \theta\right)$ and $\|c(z)\|_\infty \leq \rho\,(\epsilon + 1)$ hold. Hence, by the Harnack Inequality [23], there exists a positive constant $C_* = C_*(\|c\|_\infty, \Omega)$, such that

$$\max_{\bar{\Omega}} \eta \leq C_* \min_{\bar{\Omega}} \eta \tag{19}$$

Now, if $\eta(z_0) = \max_{\bar{\Omega}} \eta$ and $\theta(z_0) = \max_{\bar{\Omega}} \theta$, then again by the Maximum Principle Theorem, it follows:

$$\epsilon\frac{\eta(z_0)}{\theta(z_0)} \geq 1 + \eta(z_0) > 1.$$

Recalling that $\theta \leq 1$ in $\bar{\Omega}$, one has $\max_{\bar{\Omega}} \eta > \dfrac{1}{\epsilon}$. Hence, from (19) it follows:

$$\min_{\bar{\Omega}} \eta \geq \frac{1}{\epsilon C_*}.$$

By applying again the Maximum Principle Theorem to (18.2), if $\eta(z_1) = \min_{\bar{\Omega}} \eta$ and $\theta(z_1) = \min_{\bar{\Omega}} \theta$, then

$$1 - \theta(z_1) - \frac{\theta(z_1)}{\epsilon} 2^{(1-\epsilon\eta(z_1))} \leq 0$$

so that

$$\min_{\bar{\Omega}} \theta \geq \frac{\epsilon}{\epsilon + 2^{(1-\epsilon \min_{\bar{\Omega}} \eta)}} \geq \frac{\epsilon}{\epsilon + 2}$$

As a consequence, $\dfrac{\epsilon}{\epsilon + 2} \leq \theta \leq 1$ in $\bar{\Omega}$ holds. It is worth noting that the lower bound for θ is indeed the steady state value of the non trivial equilibrium E_2 in (7) discussed in the previous sections.

3. **Turing instability and pattern formation.** In this section, using linear stability analysis, we perform analytical investigations on system (3) to show the occurrence of spatial patterns induced by diffusion, i.e. the *diffusion-driven* or *Turing instability phenomenon*. We recall that a reaction-diffusion system exhibits diffusion-driven instability, if a homogeneous steady state is *stable* to small perturbations in the absence of diffusion, but it is *unstable* to small spatial perturbations when diffusion is present [30].

3.1. **Linear stability analysis.** As far as diffusion-driven instability is concerned, linear stability analysis is considered a useful technique to obtain conditions - expressed in terms of the system parameters - for the arising of instability and to determine the characteristic length of the resulting spatial pattern. In the following we briefly recall such conditions. We start by considering the general reaction diffusion system

$$\frac{\partial w}{\partial t} = D\Delta w + F(w) \tag{20}$$

with zero flux boundary conditions on a 2D domain. In (20)

$$w = \begin{pmatrix} \eta \\ \theta \end{pmatrix}, \qquad D = \begin{pmatrix} 1 & 0 \\ 0 & d \end{pmatrix}, \qquad F = \begin{pmatrix} f(\eta,\theta) \\ g(\eta,\theta) \end{pmatrix},$$

i.e. w contains the system variables, D contains the diffusion coefficients and F accounts for the reaction kinetics.

The homogeneous equilibrium $E = w_e = (\eta_e, \theta_e)$ verifies $F(w_e) = 0$ and its stability can be analyzed by studying the behavior of the system when a small inhomogeneous perturbation δw is introduced in the neighborhood of w_e, i.e. $w = w_e + \delta w$. The perturbation δw can be written in terms of its spectral decomposition given by:

$$\delta w(z,t) = \sum_j c_j e^{\lambda_j t} e^{-i\mathbf{k}\cdot\mathbf{z}}, \tag{21}$$

where $\mathbf{k} = (k_1, k_2)$ is the wave number vector and $\mathbf{z} = (x, y)$ the spatial variable. Hence, the wave modes k_j rule the spatial part whereas the related eigenvalues $\lambda_j = \lambda(k_j)$ account for the temporal part and describe the growth rate of the perturbation. By substituting (21) in (20) and retaining only the linear terms, one obtains for each k_j the equation:

$$\left|\lambda_j I - J(\eta_e, \theta_e) + Dk_j^2\right| = 0,$$

where $J(\eta_e, \theta_e)$ is the Jacobian matrix evaluated at the steady state E. Such equation provides the characteristic polynomial of (20):

$$\lambda^2 + \left[k^2(1+d) - tr(J(\eta_e, \theta_e))\right]\lambda + h(k^2) = 0, \tag{22}$$

with

$$h(k^2) = k^4 d - k^2(J_{22}^e + dJ_{11}^e) + det(J(\eta_e, \theta_e)).$$

To predict the unstable wave numbers one makes use of the dispersion relation $\lambda(k)$, obtained by solving (22). The growing modes look like $We^{i\mathbf{k}\cdot\mathbf{z}}e^{\lambda(k)t}$, where W is the amplitude and $\lambda(k)$ is the growth rate defined by the dispersion relation. Hence, those wave numbers k characterized by $Re(\lambda(k)) > 0$ will grow exponentially whereas those such that $Re(\lambda(k)) < 0$ will decay.

An estimate of the most unstable wave number may be achieved by considering that, at the onset of instability, $\lambda(k_c) = 0$ holds. Thus, from (22), one obtains the critical wavenumber:

$$k_c^2 = \frac{J_{22}^e + d_c J_{11}^e}{2d} = \sqrt{\frac{det(J(\eta_e, \theta_e))}{d_c}} \tag{23}$$

and the related characteristic length of the pattern, $\lambda_c = \dfrac{2\pi}{k_c}$. Here J_{ij}^e stands for the ij entry of the Jacobian matrix evaluated at the equilibrium $E = (\eta_e, \theta_e)$.

For the general system (20), it can be easily shown that the Turing space - consisting of parameters resulting in Turing instability - is bounded by the following inequalities:

$$\begin{cases} J_{11}^e + J_{22}^e < 0 \\ J_{11}^e J_{22}^e - J_{12}^e J_{21}^e > 0 \\ dJ_{11}^e + J_{22}^e > 0 \\ \dfrac{(J_{22}^e + dJ_{11}^e)^2}{4d} > det(J(\eta_e, \theta_e)) \end{cases} \tag{24}$$

The first two inequalities are derived by stability considerations on the homogeneous equilibrium E in the absence of diffusion, the others are obtained, as (23), by considerations on the onset of instability when diffusion is introduced. We refer to [30] and references therein for the explicit derivation of (24).

Taking into account such general conditions, we turn to the electrodeposition model (3). For this model, the spatially homogeneous equilibria are given by: $E_1 = (\eta_1, \theta_1) = \left(0, \dfrac{\epsilon}{\epsilon + 2}\right)$ and $E_2 = (\eta_2, \theta_2) = \left(\dfrac{1}{\epsilon}, \dfrac{\epsilon}{\epsilon + 1}\right)$.

As shown in Sec.2, the homogeneous equilibrium E_1 is stable for every value of the parameters. Even when diffusion is present, the necessary condition for Turing instability is never satisfied, being $dJ_{11}(E_1) + J_{22}(E_1) < 0$.

Differently, the spatially uniform steady state E_2 may undergo diffusion driven instability. Recalling (14), the set of conditions for diffusion-driven instability is given by:

$$\begin{cases} \rho\epsilon^3 - \sigma A e^{\alpha_0} (\epsilon + 1)^3 < 0 \\ A\sigma e^{\alpha_0} (ln2 - \epsilon) > 0 \\ d\rho\epsilon^3 - \sigma A e^{\alpha_0} (\epsilon + 1)^3 > 0 \\ \left[\dfrac{d\rho\epsilon^3 - \sigma A e^{\alpha_0} (\epsilon + 1)^3}{\epsilon (\epsilon + 1)^2}\right]^2 - \dfrac{4d\rho\sigma A e^{\alpha_0} (ln2 - \epsilon)}{\epsilon + 1} > 0 \end{cases} \tag{25}$$

where $\alpha_0 = \dfrac{a\epsilon + a + b\epsilon^2}{\epsilon (\epsilon + 1)}$. Since these inequalities involve the model parameters, they allow us to locate a region in the parameter space such that E_2 is stable to small perturbations in the absence of diffusion, but it can be unstable to small spatial perturbations when the diffusion parameter d is non-zero and greater than a critical value d_c.

When the other parameters are fixed, d_c can be determined by combining the third and fourth conditions in the set of inequalities (25).

According to the phase-plane analysis performed in Sec.2, we stress that the model (3) exhibits more than one stable homogeneous steady state. As widely shown in literature - see e.g. [16] and references therein - reaction-diffusion systems with such a kinetic, turn out to be particularly important for the applications and can generate even more complex patterns since initial conditions are here particularly relevant. In the present case, the trivial equilibrium E_1 is always stable and then the Turing spatial patterns only may arise by the destabilization, due to infinitesimal spatial perturbations, of the stable homogeneous equilibrium E_2. To study the arising of spatial patterns we have to identify a set of parameters making the equilibrium E_2 stable in absence of diffusion.
For example, taking the same numerical values as in Sec.2, i.e. $\epsilon = 0.5$, $\rho = 40$, $\sigma = 2$, $a = 1$, $b = 1$, and considering A and d as bifurcation parameters, it is easy to show that the conditions (25) are verified for $A > A_c = 0.07183$ and for d satisfying the following inequalities:

$$d > 13.92A, \qquad \varphi_2\, d^2 - \varphi_1\, A\, d + \varphi_0\, A^2 > 0, \tag{26}$$

where $\varphi_2 = 4.93827$, $\varphi_1 = 243.72524$, $\varphi_0 = 957.08407$. For example, by choosing the parameter A so that $A = 0.2 > A_c$, for the arising of spatial patterns, the diffusion parameter d has to be greater than $d_c = 9.1$.

3.2. **Numerical simulations and comparisons with experiments.** In two space dimensions, the most typical patterns for Turing systems turn out to be stripes or hexagonally arranged spots, even if in some cases different typologies have been observed as rhombic or labyrinthine patterns [21]. To predict the spatial characteristics of the resulting patterns, linear analysis is not enough since pattern selection is governed by complicated nonlinear dynamics. To this aim, theoretical investigations must rely on nonlinear bifurcation analysis and on the use of the amplitude equations formalism, see i.e. [12, 13, 14, 31]. This kind of analysis, however, goes beyond the scope of the present paper, so that we investigate numerically the aspects related to pattern selection. Here we present numerical simulations of the model and some comparisons with electrodeposition experiments. These experiments and the acronyms used in the following discussion are briefly described in the Appendix. To solve the reaction-diffusion system (19) on the rectangular spatial domain $[0, L_1] \times [0, L_2]$ for the times $t \in [0, T]$, we apply the Comsol Multiphysics package [11] based on the finite element method in space. To have accurate simulations both in space and time, able to capture the main features of the spatial patterns expected, we use a sufficiently fine mesh (almost 35000 degrees of freedom) and we select as time integrator the BDF (implicit) schemes of high order (up to five). Numerical simulations, have been performed in the domain $[0, 100] \times [0, 70]$ and by considering a spatially distributed random infinitesimal perturbation around the non trivial stationary state E_2. We fix the parameters of the system such that: $\epsilon = 0.5$, $\rho = 40$, $\sigma = 2$, $b = 1$, $A = 0.2$, $d = 10$ and vary a in order to outline its role in pattern selection. The motivation for this choice is based on both structural and experimental evidences.

Under the physico-chemical approximations adopted to write model (3) - in particular as far as the source term for the morphology equation $(3)_1$ is concerned, the variable η - having primarily the meaning of dimensionless morphology - is essentially proportional to the local overvoltage, driving the electrodeposition process out of equilibrium. With this proviso, the electrochemical meaning of the parameter a is essentially the inverse of the electron-tunneling barrier that has to be overcome by

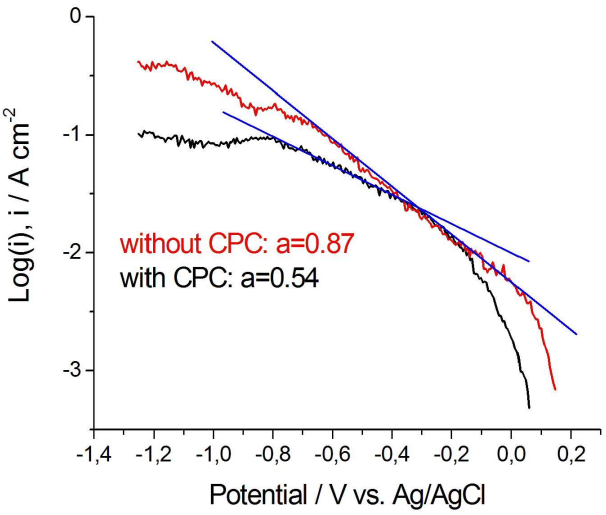

FIGURE 3. Potentiodynamic curves recorded at a Ni-P electrode in contact with Au-Cu baths, without and with added CPC 100 ppm. The Tafel slope estimates a are deduced from the exponential portion of the curves.

electrons tunneling from the electrode into the electrolyte to reduce metal adatom precursors (e.g. [18]). Low values of a thus correspond to inhibited electron tunneling resulting in a lower rate of adatom formation, eventually giving rise to a lower surface concentration of adatoms that have a better chance to diffuse to low-energy sites, giving rise to a more stable morphology, exhibiting less singularities. From the experimental point of view, lower a values can be obtained by adding special chemicals to the electrodeposition solutions.

In fact, the relationship between space-averaged and the average growth rate i can be measured: in Fig.3 we report measured current i vs potential (with respect to $Ag/AgCl$) curves - and the corresponding estimates of a - from the electrochemical processes that gave rise to the growth of the deposits whose SEM micrographs are shown in Fig.7 and Fig.8. Of course, higher growth rates correspond to more unstable (i.e. a situation like Fig.5) morphologies (see, e.g. [32]).

Along with the above experimental arguments, also numerical simulations give evidence for the role of the parameter a in adjusting pattern selection. In order to verify conditions (25), a must vary in the range $a \in [a_{min}, a_{max}]$ where, for the chosen parameter values, $a_{min} = 0.4879$ and $a_{max} = 1.05209$.

We focus our investigations on the following features related to morphological aspects of the patterns: (i) stationary pattern typology, i.e type *spots* or type *spots and worms* (ii) transient pattern typology. By varying the parameter a, the two different typologies of patterns, encountered in experiments, are qualitatively obtained as stationary Turing patterns; on the other hand, by considering representative values of the parameter a, interesting transient patterns can arise, for example accounting for the presence of holes in the morphology.

As far as the feature (i) is concerned, we find that very low values of a, i.e. $a \cong a_{min}$ lead to a stationary Turing patterns in which coexistence between spots and worms is well established, as shown in Fig.4(a). Experiments for AuCuCd bath with KCN and BPPEI support such results as shown in Fig.4(b): here the presence of KCN (yielding a relatively high CN^- concentration) correlates with a low d value and the presence of BPPEI correlates with a low a value.

By increasing the value of a up to a_{max}, only spots survive in the stationary Turing pattern, as shown in Fig.5(a). The corresponding experimental situation is depicted in Fig.5(b) related to AuCuCd bath with KCN and without BPPEI: here the presence of KCN (yielding a relatively high CN^- concentration) correlates with low d value whereas the absence of BPPEI correlates with high a value. This kind of phenomenology encounters a general experimental evidence, in fact, as implied by the previous discussion on the physico-chemical role of parameter a, relatively high a values correspond (under otherwise identical chemical and polarisation conditions) to a high surface density of adatoms, ending up incorporated into high-energy sites, thereby causing unstable growth, eventually yielding isolated outgrowth features, such as: stalks, dendrites or piles of spheroidal crystallites, according to the specific system [32, 35]. Such outgrowth features, viewed in plane, would correspond to a pattern of isolated spots, like those in Fig.5(b). To the contrary, relatively low a values correspond to the possibility for adatoms to reach low-energy crystal sites, where they contribute to the formation of more correlated morphologies, such as terraces and islands, tending to outgrow into ridges, that would show up as *worms* in the geometry chosen for the representation of numerical data, like in Fig.4(b). On the other hand, fixing the parameter a so that $a = a_{min}$, the effect of greatly increasing d from d_c, is to obtain only spots at the stationary pattern.

The feature (ii) is discussed by looking at the transient behaviors. Along with the asymptotic regimes, also transient behaviors turn out to be of a certain relevance, especially for those modelling situations - as the present one - strictly linked with experimental systems. This is for example the case of some consumer-finite resource systems arising to model bacterial growth, whose very interesting transient behaviors surprisingly account for the complex patterns of the related experimental systems [28, 29].

For our electrodeposition model, an example for the case $a = 0.8$ and $d = 20$ is provided in Fig.6(a) to show numerical simulations of η and θ in qualitative agreement with an interesting electrodeposited surface shown in Fig.6(b) where the "overlapped" chemistry (Cu waves) and morphology (central "eye" formation) can be identified. This experimental situation corresponds to AuCuCd bath without KCN and without BPPEI: here the absence of KCN (yielding a relatively low CN^- concentration) correlates with a higher d value and the absence of BPPEI correlates with a higher a value. The above circumstance is coherent with the electrochemistry of $3D$ growth, in which outgrowth processes are self-enhancing: in fact - except in cases where levelling is obtained by chemicals that are specially designed to adsorb at high-curvature surfaces - morphological instabilities give rise to localisations in electric field, concentration gradient and surface chemistry that enhance local growth rate.

Furthermore, by considering the same numerical a and d values as the two cases in Fig.4-Fig.5, we find how suitable transient patterns interestingly account for the presence of holes in the morphology, accordingly with the related experimental situations. More precisely, in Fig.7(a) a transient pattern of morphology in the case

$a = 0.5$ and $d = 10$ is presented which qualitatively exhibits many small holes. As shown in Fig.7(b), this is consistent with the AuCu bath with CPC: here the presence of the two ligands (CN^- and EDTA) correlates with a low d value and the presence of CPC correlates with a low a value. Differently, in Fig.8(a) a transient pattern of morphology in the case $a = 0.9$ and $d = 10$ qualitatively accounts for the occurrence of few large holes. The corresponding experimental situation - AuCu bath without CPC - represented in Fig.8(b): here the presence the two ligands (CN and EDTA) correlates with a low d value whereas the absence of CPC correlates with a high a value.

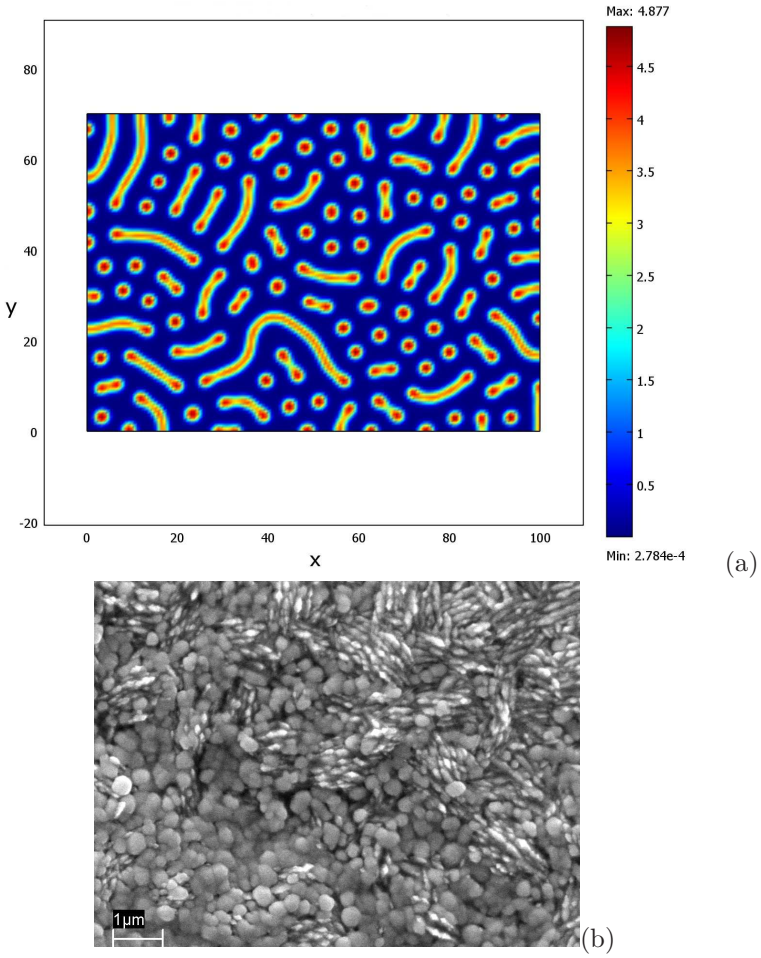

FIGURE 4. Spotty-Wormy pattern: (a) Numerical simulation of the morphology for the case $a = 0.5$ and $d = 10$. The stationary Turing pattern is depicted, exhibiting coexistence of spots and worms. (b) AuCuCd bath with KCN and BPPEI. The presence of KCN (yielding a relatively high CN^- concentration) correlates with a lower d value ($d = 10$ wrt 20). The presence of BPPEI correlates with a lower a value ($a = 0.5$ wrt 0.9).

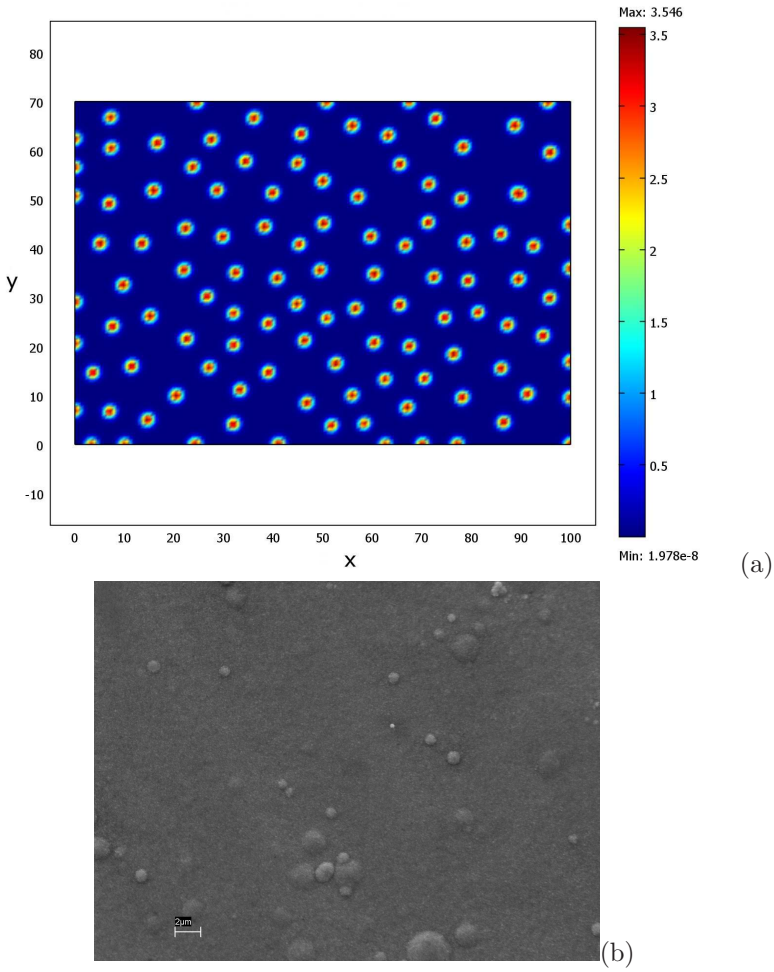

FIGURE 5. Spotty pattern: (a) Numerical simulation of the morphology for the case $a = 0.9$ and $d = 10$. The stationary Turing spotty pattern is shown. (b) AuCuCd bath with KCN and without BPPEI. The presence of KCN (yielding a relatively high CN^- concentration) correlates with a lower d value ($d = 10$ wrt 20). The absence of BPPEI correlates with a higher a value ($a = 0.9$ wrt 0.5).

4. **Concluding remarks.** We considered a reaction-diffusion system in order to model metal growth processes within the electrodeposition context, focussing on morphological pattern formation in a finite two-dimensional spatial domain. We studied the nonlinear dynamics of the system from both theoretical and numerical points of view. The obtained results were thus compared with some experiments for the electrodeposition of $Au - Cu$ and $Au - Cu - Cd$ alloys. Two major points were addressed: (i) bifurcations in the spatially homogeneous case (ii) diffusion-driven pattern formation and pattern selection. System analysis stressed the crucial role of specific parameters for stability and selection of solutions.

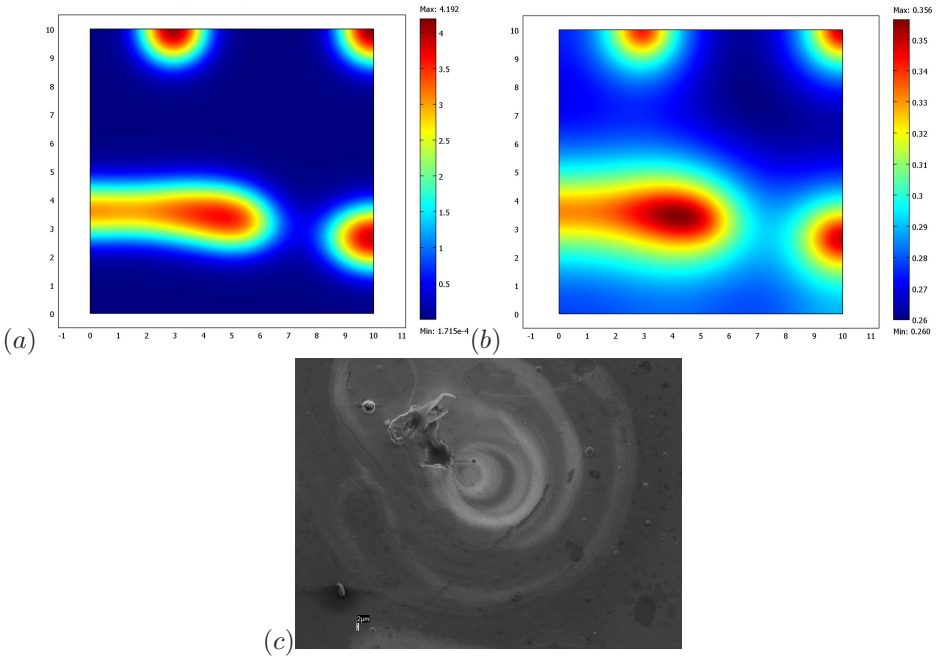

FIGURE 6. Morphology & Chemistry. Numerical simulations of (a) morphology η and (b) chemistry θ for the case $a = 0.8$ and $d = 20$. A transient Turing pattern is shown. (c) AuCuCd bath without KCN and without BPPEI. The absence of KCN (yielding a relatively low CN^- concentration) correlates with a higher d value ($d = 20$ wrt 10). The absence of BPPEI correlates with a higher a value ($a = 0.8$ wrt 0.5).

More precisely, dealing with the point (i), we recognized the parameter A as responsible for the change of stability of the homogeneous non trivial equilibrium E_2 and also we detected the occurrence of a subcritical Hopf bifurcation when A passes through the threshold value A_c. The stabilizing role of A in the range $A > A_c$ was confirmed from the chemical point of view. In fact the chemically stabilizing factor is the coverage of the Au surface with CN^- and when the attachment efficiency A is below a threshold A_c - dictated by both material properties and reaction rate - instability in the growth dynamics is enhanced because of the accumulation of CN^-.

Concerning the point (ii), we obtained a set of conditions - in terms of the system parameters - ensuring the initiation of spatial patterns induced by diffusion. At this aim - accordingly to its chemical meaning - the diffusion parameter d was shown to be essential for the arising of instability and the appearing of spatial patterns.

Our study also revealed the peculiar function of the parameter a - essentially representing the inverse of the electron-tunneling barrier that has to be overcome by electrons tunneling from the electrode into the electrolyte to reduce metal adatom precursors - in adjusting pattern selection. Fixing $d \approx d_c$, we found that lower values of the parameter a caused a coexistence between different pattern typologies, i.e.

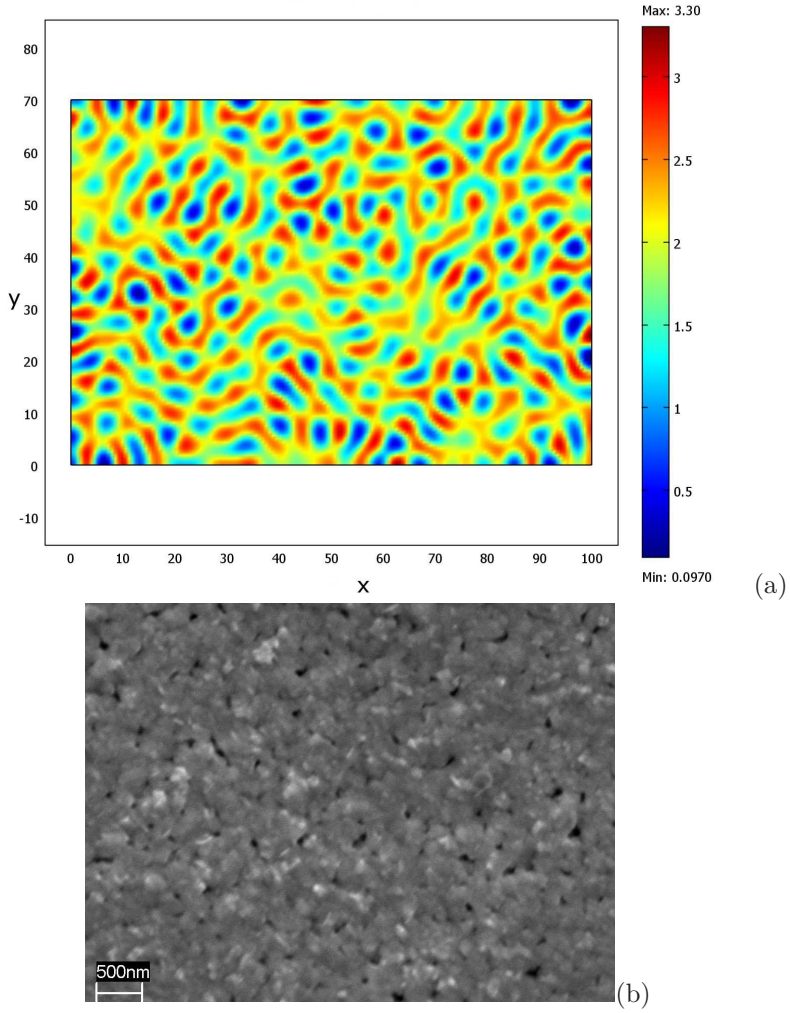

FIGURE 7. Type Holes: (a) Numerical simulation of the morphology for the case $a = 0.5$ and $d = 10$. The transient behavior of the system is depicted, qualitatively exhibiting many small holes. (b) AuCu bath with CPC. The presence of the two ligands (CN^- and EDTA) correlates with a lower d value ($d = 10$ wrt 20). The presence of CPC correlates with a lower a value ($a = 0.5$ wrt 0.9).

spotty and wormy patterns, whereas higher values of the parameter a resulted only in spotty patterns.

Such a phenomenology is supported by physico-chemical evidence: in fact, the presented experiments have displayed that relatively high a values are related to isolated outgrowth features such as: stalks, dendrites or piles of spheroidal crystallites, that - viewed in plane - would correspond to a pattern of isolated spots. Differently, low a values correspond to more correlated morphologies, such as terraces and islands, tending to outgrow into ridges, that would appear as *worms* in the geometry chosen for the representation of numerical data.

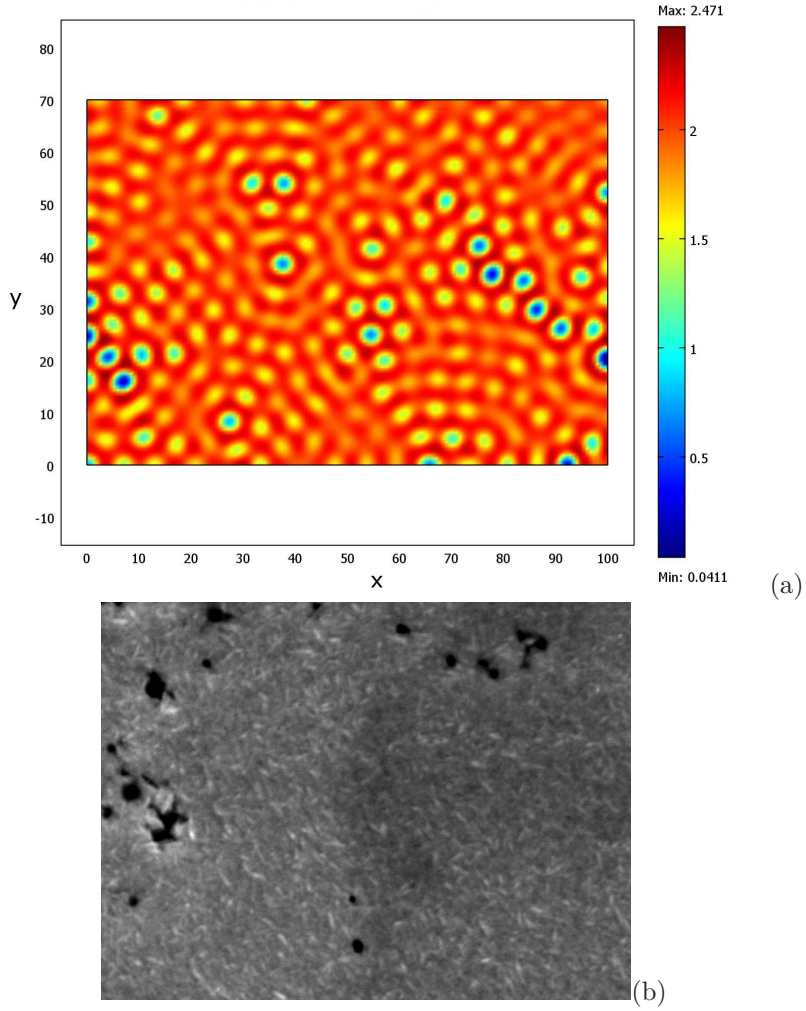

FIGURE 8. Type Holes: (a) Numerical simulation of the morphology for the case $a = 0.9$ and $d = 10$. The transient behavior of the system is depicted, qualitatively exhibiting few large holes. (b) AuCu bath without CPC.The presence the two ligands (CN and EDTA) correlates with a lower d value ($d = 10$ wrt 20). The absence of CPC correlates with a higher a value ($a = 0.9$ wrt 0.5).

The fact that we could identify the impact of the numerical values of specific electrokinetic parameters on the dynamics of morphological evolution and, in particular, on the selection of morphological patterns has a major bearing to the field of electrochemical metal growth. In fact, such numerical values can be obtained by tailoring the bath chemistry and choosing/designing suitable additive molecules. Furthermore, since such parameters can - in principle - be both measured and transduced, it is possible to employ the dynamical models we developed in this work also in closed-loop control schemes for industrial metal-plating processes.

5. **Appendix.** In this study we considered two types of cyanide-based baths for the electrodeposition of 18 kt Au-alloys: AuCu, more suitable for red gold and Hamilton decorative finishes and AuCuCd, a typical electroforming bath. These baths consist in a metal source, in this case cyanide salts of the three relevant metals and two types of additives: (i) free complexing agent (CN^-, EDTA), typically used to extend the bath life, that can be jeopardised by loss of the complexing agent by environmental oxidation and (ii) organic levellers, in our case cetylpyridinium chloride (CPC) and benzyl-phenyl polyethylene imine (BPPEI) (for details, see [6]).

The composition and operating conditions of the alloy electrodeposition baths are reported below. I.*AuCu bath*: Au^+ (as $KAu(CN)_2$) 7.5 g L^{-1}, Cu^{2+} (as CuO) 2.5 g L^{-1}, EDTA 11.5 g L^{-1}, citric acid 40 g L^{-1}, ammonium citrate 40 g L^{-1}, pH 6, room temperature, current density 20 mA cm^{-2}. As a leveller we added CPC 100 ppm. II. *AuCuCd bath*: Au^+ (as $KAu(CN)_2$) 2.5 g L^{-1}, Cu^+ (as $K_2Cu(CN)_3$) 60 g L^{-1}, Cd^{2+} (as $KCd(CN)_3$) 2.5 g L^{-1}, pH 11, $T = 70^oC$, current density 10 mA cm^{-2}. In the case of addition of the free-cyanide bath, KCN 25 g L^{-1} was added. As a leveller we added 10 ppm of BPPEI.

These two additives have two chief types of effect on interfacial electrochemistry. Cyanide is strongly adsorbed at the growing surface, thus affecting adatom diffusivity (see, e.g. [3]). In terms of our model, higher CN concentrations in the bath thus give rise to a reduction of D^*_{sc}, that - if $D^*_s \approx const$ - of course implies a reduction of d.

The leveller typically forms an interfacial organic film between the metallic surface and the aqueous electrolyte, generally (some exceptions are related to the existence of resonance tunneling processes [15]) providing an additional barrier - with respect to a compact layer of water - to electron tunneling from the metal to the electroactive metal cation. Within the framework of quantum chemical kinetics, this can be viewed as a decrease of the phenomenological electrokinetic parameter a.

REFERENCES

[1] B. Bozzini, G. Giovannelli and P. L. Cavallotti, *Investigation into the electrodeposition of Au-Cu-matrix particulate composites*, J. Appl. Electrochem., **29** (1999), 685–692.

[2] B. Bozzini, G. Giovannelli, C. Lenardi, M. Serra and M. Placidi, "Effects of Organic Additives on Morphological Evolution of Electrodeposited Au Alloys," ECS Proceeding Volume PV 2001-08 (ISBN 1-56677-324-8) - Morphological Evolution of Electrodeposits and Electrochemical Processing in ULSI fabrication and Electrodeposition of and on Semiconductors IV. K. Kondo, D.P. Barkey, J. C. Bradley, F Argoul, P. C. Andricacos and J. L. Stickney Ed.s, - p. 85.

[3] B. Bozzini and A. Fanigliulo, *Effects of Tl on the electrocrystallisation of thick Au layers from $KAu(CN)_2$ solutions*, J. Cryst. Growth, **243** (2002), 190–203.

[4] B. Bozzini, G. Giovannelli, S. Natali, A. Fanigliulo and P. L. Cavallotti, *Crystallographic structure of gold films electrodeposited at low current densities*, J. Mat. Sci., **37** (2002), 3903–3913.

[5] B. Bozzini, P. L. Cavallotti and G. Giovannelli, *Electrokinetic behavior of gold alloy and composite plating baths*, Met. Fin., **100** (2002), 50–60.

[6] B. Bozzini, L. D'Urzo and C. Mele, *A novel polymeric leveller for the electrodeposition of copper from acidic sulphate bath: a spectroelectrochemical investigation*, Electrochim. Acta, **52** (2007), 4767–4777.

[7] B. Bozzini, I. Sgura and L. D'Urzo, "Modelling of Morphological Control of Electrodeposited Cu by Adsorption of Aminoacids and Oligopeptides," in: New Developments in Electrodeposition and Pitting Research, edited by A. El Nemr, Research Signpost Pub., Fort P.O., Trivandrum-695 023, Kerala, India, 2007.

[8] B. Bozzini, G. Giovannelli and C. Mele, *Electrochemical dynamics and structure of the Ag/AgCl interface in chloride-containing aqueous solutions*, Surf. & Coat. Technol., **201** (2007), 4619–4627.

[9] B. Bozzini, D. Lacitignola and I. Sgura, *A reaction-diffusion model of spatial pattern formation in electrodeposition*, J. of Physics: Conference Series **96** (2008), 012051.

[10] B. Bozzini, D. Lacitignola and I. Sgura, *Travelling waves in a reaction-diffusion model for electrodeposition*, Math. Comp. in Simulat., (in press).

[11] COMSOL MULTIPHYSICS v.3.5 User's guide (2008).

[12] T. K. Callahan and E. Knobloch, *Pattern formation in three-dimensional reaction-diffusion systems*, Physica D, **132** (1999), 339–362.

[13] J. D. Crawford, *Introduction to bifurcation theory*, Rev. Mod. Phys., **63** (1991), 991–1037.

[14] G. Dewel, P. Borckmans, A. D. Wit, B. Rudovics, J. Perraud, E. Dulos, J. Boissonade and P. D. Kepper, *Pattern selection and localized structures in reaction-diffusion systems*, Physica A, **213** (1995), 181–198.

[15] E. E. Farndon, F. C. Walsh and S. A. Campbell, *Effect of thiourea, benzotriazole and 4,5-dithiaoctane-1,8-disulphonic acid on the kinetics of copper deposition from dilute acid sulphate solutions*, J. Appl. Electrochem., **25** (1995), 574–583.

[16] E. Finke and D. Simon, *On the presence of spatial pattern formation in a bistable dynamical system*, Appl. Phys. A, **60** (1995), 487–495.

[17] P. Glansdorff and I. Prigogine, "Thermodynamic Theory of Structure, Stability and Fluctuations," Wiley-Interscience, 1971.

[18] J. Goodisman, "Electrochemistry: Theoretical Foundations," J. Wiley & Sons, 336–364, 1987.

[19] J. Guckenheimer and P. Holmes, "Nonlinear Oscillations Dynamical Systems and Bifurcations of Vector Fields," Applied Mathematical Sciences, **42**, Springer-Verlag, New York, 1983.

[20] J. L. Hudson and T. T. Tsotis, *Electrochemical reaction dynamics: A review*, Chem. Eng. Sci., **49** (1994), 1493–1572.

[21] R. Kapral, K. Showalter, "Chemical Waves and Patterns," Kluwer Academic Publishers, 1995.

[22] K. Krischer, B. E. Conway, J. O. Bockris and R. White, Editors, "Modern Aspects of Electrochemistry," Plenum, New York, 1999.

[23] C. S. Lin, W. M. Ni and I. Takagi, *Large amplitude stationary solutions to a chemotaxis system*, J. Diff. Equ., **72** (1988), 1–27.

[24] Y. Lou and W. M. Ni, *Diffusion, self-diffusion and cross-diffusion*, J. Diff. Equ., **131** (1996), 79–131.

[25] P. K. Maini, K. J. Painter and H. N. P. Chau, *Spatial pattern formation in chemical and biological systems*, Faraday Transactions, **93** (1997), 3601–3610.

[26] P. K. Maini and H. G. Othmer, "Mathematical Models for Biological Pattern Formation," The IMA Volumes in Mathematics and its Applications - Frontiers in Applications of Mathematics, Vol. **121**, Springer, 2001. ISBN: 0387951032.

[27] P. K. Maini, *Using mathematical models to help understand biological pattern formation*, Comptes Rendus Biologies, **327** (2004), 225–234.

[28] M. Mimura, H. Sakaguchi and M. Matsushita, *Reaction-diffusion modelling of bacterial colony patterns*, Physica A, (2000), 282–283.

[29] M. Mimura, *Pattern formation in consumer-finite resource reaction-diffusion systems*, Publ. RIMS, Kyoto Univ., **40** (2004), 1413–1431.

[30] J. D. Murray, "Mathematical Biology II; Spatial Models and Biomedical Applications," 3rd edition,Interdisciplinary Applied Mathematics, **18**, Springer-Verlag, New York, 2003. xxvi+811 pp. ISBN: 0-387-95228-4.

[31] A. C. Newell, T. Passot and J. Lega, *Order parameter equations for patterns*, Annu. Rev. Fluid Mech., **25** (1993), Annual Reviews, Palo Alto, CA, 399–453.

[32] K. I. Popov, S. S. Djokic and B. N. Grgur, "Fundamental Aspects of Electrometallurgy," Klower, N.Y., 29–95, (2002).

[33] P. Schilardi, S. Méndez, R. C. Salvarezza and A. J. Arvia, *Evolution of the growth front for copper electrodeposition followed by real time imaging*, Langmuir, **14** (1998), 4308–4314.

[34] A. M. Turing, *The chemical basis of morphogenesis*, Philosophical Transactions of the Royal Society of London B, Biological Sciences, **237** (1952), 37–72.

[35] R. Winand, *Electrocrystallization - theory and applications*, Hydrometallurgy, **29** (1992), 567–598.

Received May 8, 2009; Accepted December 24, 2009.

E-mail address: (corresponding author) deborah.lacitignola@unisalento.it
E-mail address: benedetto.bozzini@unisalento.it;ivonne.sgura@unisalento.it